Hindawi Publishing Corporation
International Journal of Antennas and Propagation
Volume 2012, Article ID 102495, 7 pages
doi:10.1155/2012/102495

Research Article

Evaluation of the Inductive Coupling between Equivalent Emission Sources of Components

Moisés Ferber,[1] Sanâa Zangui,[1] Carlos Sartori,[2] Christian Vollaire,[1] Ronan Perrussel,[3] and Laurent Krähenbühl[1]

[1] *Laboratoire Ampère, CNRS UMR5005, Ecole Centrale de Lyon, Université de Lyon, 69130 Ecully, France*
[2] *Laboratorio de Eletromagnetismo Aplicado, Universidade de São Paulo, 05508900 São Paulo, SP, Brazil*
[3] *LAPLACE, CNRS UMR5213, INP-ENSEEIHT, Université de Toulouse, 31071 Toulouse, France*

Correspondence should be addressed to Moisés Ferber, moisesferber@gmail.com

Received 13 August 2011; Accepted 17 October 2011

Academic Editor: Dragan Poljak

Copyright © 2012 Moisés Ferber et al. This is an open access article distributed under the Creative Commons Attribution License, which permits unrestricted use, distribution, and reproduction in any medium, provided the original work is properly cited.

The electromagnetic interference between electronic systems or between their components influences the overall performance. It is important thus to model these interferences in order to optimize the position of the components of an electronic system. In this paper, a methodology to construct the equivalent model of magnetic field sources is proposed. It is based on the multipole expansion, and it represents the radiated emission of generic structures in a spherical reference frame. Experimental results for different kinds of sources are presented illustrating our method.

1. Introduction

The development of semiconductor technology in the last decades has greatly increased the use of power electronics in various applications, such as computer power supplies, voltage converters, electronic ballasts, and variable-speed drives [1]. Recently, new applications of power electronics have also appeared in the vehicle industry, such as electric cars and airplanes. However, the commutation of the switches (rectifiers, SCRs and triacs, BJTs, MOSFETs, and IGBTs) generates high currents with high di/dt, and, thus, a wide bandwidth of unwanted electromagnetic interference (EMI) pollutes the electromagnetic environment [2].

The electromagnetic compatibility (EMC) is an engineering domain responsible to ensure that systems, equipment, and devices can coexist satisfactorily in the same electromagnetic environment [3]. Electric cars, for instance, may encounter malfunction in its electronic systems (ESP, ABS, ALS, etc) if special care is not taken. The EMI between the cables of the power electronics and the cables carrying electronic signals, if they are too close to each other without proper shielding, may prevent the correct operation of certain systems [4].

There are not many reliable methods to predict the EMC of a complex system in the design phase [5], and, thus, in practice, the EMC design is still carried out by trial and error [3] causing high development cost in case of malfunctioning due to EMI, when the prototype is tested.

To ensure the compatibility of cables, equipment, and systems at the design phase, EMC predictive tools must be improved [5]. In order to achieve this requirement, frequency domain simulations can be performed utilizing equivalent models for the EMI sources. For instance, in power electronics, the range of frequency analyzed can be restricted from 10 kHz to 50 MHz, which comprises the common operating range of semiconductor switches utilized in power converters and frequency harmonics produced by them.

The EMI is usually established in different ways, for zinstance, the near-field coupling between filter components [6–9] or the coupling between wires [10]. Each coupling phenomenon is thus best modeled by different mathematical models.

The near-field coupling between filter components can be well modeled by a methodology based on the multipole

expansion, which represents the radiation emission in a spherical reference system (r, θ, φ) [6–9], whereas the coupling between wires is usually well modeled by the PEEC method [10].

This paper presents a methodology to determine the first two coefficients of the multipole expansion (Q_{10} and Q_{20}) of a generic magnetic field source, by a numerical or an experimental approach, depending upon the complexity of the source. The numerical approach is rather limited to simple sources, but the experimental approach has no limitations over the geometrical complexity of the source.

The experimental approach utilizes an antenna consisting of four loops around the magnetic field source. The mutual coupling between the loops must be taken into account when modeling the source, in order to avoid a significant error, which can be up to 40%.

Finally, the methodology is validated by comparing the calculated and measured mutual inductance of a modeled power transformer and a well-known loop.

2. Theory of Multipole Expansion

The multipole expansion can be used to represent electromagnetic fields in 3D, assuming that the field is computed outside a sphere of a given radius that contains the equivalent source. Figure 1 shows the reference sphere considered [11].

In the case of outgoing radiated emission sources, the multipole expansion allows expressing the electric and magnetic fields as [12]

$$E(r,\theta,\varphi) = \sum_{n=1}^{\infty}\sum_{m=-n}^{n} Q_{nm}^{\mathrm{TE}}\mathbf{F}_{1nm}(r,\theta,\varphi) + Q_{nm}^{\mathrm{TM}}\mathbf{F}_{2nm}(r,\theta,\varphi),$$

$$H(r,\theta,\varphi) = \frac{j}{\eta}\sum_{n=1}^{\infty}\sum_{m=-n}^{n} Q_{nm}^{\mathrm{TM}}\mathbf{F}_{1nm}(r,\theta,\varphi) + Q_{nm}^{\mathrm{TE}}\mathbf{F}_{2nm}(r,\theta,\varphi), \quad (1)$$

where

(i) $\eta = \sqrt{\mu/\varepsilon}$ is the intrinsic impedance of the considered environment;

(ii) Q_{nm}^{TE} and Q_{nm}^{TM} are the magnetic and electric coefficients, respectively. The coefficients Q_{nm}^{TE} describe the strength of the transverse-electric (TE) components of the radiated field, while coefficients Q_{nm}^{TM} describe the strength of the transverse-magnetic (TM) components. Each of them corresponds to the equivalent radiated source. Thus, these coefficients are the parameters to be identified that characterize the equivalent model of the radiated field components;

(iii) $\mathbf{F}_{1nm}$ and $\mathbf{F}_{2nm}$ are the vector spherical harmonics which are solutions of Maxwell's equations in free space, excluding the sphere that involves the sources;

(iv) n is the degree, and m is the azimuthal order.

In our study, only the magnetic source in the near-field is considered. That is $Q_{nm}^{\mathrm{TM}} = 0$, and it is assumed that the electric field component is low when compared with the magnetic field. Thus, the computation of the Q_{nm}^{TE}, wrote as Q_{nm} in (2), is carried out by the radial component H_r, in near field [12, 13]:

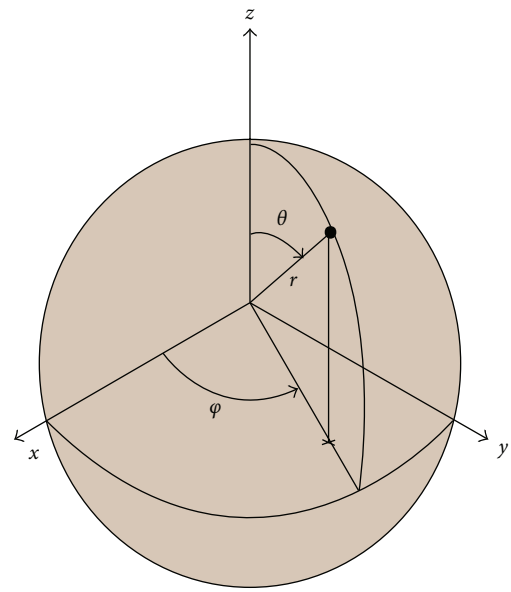

Figure 1: Reference adopted in the field computation.

$$H_r = -\frac{1}{4\pi}\sum_{n=1}^{+\infty}\sum_{m=-n}^{n} Q_{nm}\frac{\partial}{\partial r}\left(\frac{1}{r^{n+1}}\right)Y_{nm}(\theta,\varphi), \quad (2)$$

where Y_{nm} are the normalized spherical harmonics given by the following expression:

$$Y_{nm}(\theta,\varphi) = \sqrt{\frac{(2n+1)(n-m)!}{4\pi(n+m)!}}P_n^m(\cos\theta)e^{jm\varphi}. \quad (3)$$

One of the main properties of the multipole expansion to be emphasized is the decrease of the terms of order n with $r^{-(n+1)}$. This ensures a hierarchy between each order of the decomposition. The larger is the distance to the source, the fewer are the terms required to reconstruct the field. Thus, the accuracy of the mutual inductance computation is related to the choice of the maximum order description, noted $N_{\max}$. It should be observed that there are $(2n + 1)$ components for each n order. For an order source equal to $N_{\max}$, it will correspond to $N_{\max}(N_{\max} + 2)$ components, but due to the previously mentioned property (hierarchy between each order), $N_{\max}$ can be limited to 5, based on the present experience of the authors.

3. Multipole Identification

3.1. Numerical Approach. This approach consists in identifying the source utilizing the software Flux2D based on the finite element method. The software calculates the radial component of the magnetic induction on a measurement sphere S_M, which contains the source, as shown in Figure 2. The computation of the Q_{nm} coefficients is achieved by integrating these components on S_M.

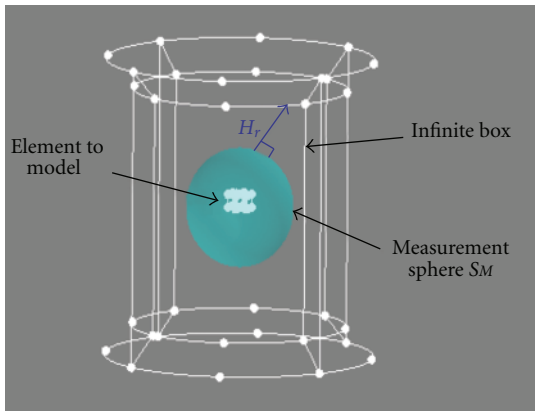

Figure 2: Source modeling Flux2D.

The coefficients of the multipole expansion can be deduced from (2), based on the following expression:

$$Q_{nm} = 4\pi \frac{r_0^n}{(n+1)} \int_0^{2\pi} \int_0^{\pi} H_r(r_0, \theta, \varphi) Y_{nm}(\theta, \varphi) dS, \quad (4)$$

where H_r corresponds to the radial component of the magnetic field on the sphere S_M of a radius of r_0. This result is due to the orthogonal property of Y_{nm} base:

$$\iint_{S_M} Y_{nm} Y_{n'm'} dS = \begin{cases} r_0^2, & \text{if } (n,m) = (n',m'), \\ 0, & \text{otherwise.} \end{cases} \quad (5)$$

The order of the approximation is not limited for this identification method. However, the computational time increases with the order. Moreover, the discretization of the sphere surface must respect the Shannon theorem in order to avoid spatial aliasing. For instance, with $n = 1$, the axes theta and phi require at least two points each, whereas, for $n = 2$, four points are required. For $n = N_{\max}$, $2N_{\max}$ points are necessary for each axis.

The numerical approach can be excessively time consuming or require too much memory, if the modeled source is geometrically complex. The experimental approach is thus an alternative, and it is suitable for practically any source.

3.2. Experimental Approach. This approach consists in identifying the source utilizing an antenna and a measurement equipment. Figure 3 shows the prototype antenna with its loop sensors corresponding to the dipole (2 loops for the dipole component Q_{10}), the quadrupole (2 loops for the quadrupole Q_{20}), and the loop from the standard CISPR16-1. All mentioned loops were built initially only in the z-direction. The complete measurement setup is surrounded by a sphere of radius r_M equal to 0.225 m. The short-circuited loops were proposed as sensors with a flat response within the 9 kHz–30 MHz frequency range. Although the use of short-circuited loops corresponds to high values of currents and thus high sensitivity, the magnetic coupling between them imposes some constraints to the measurement and calibration methodology.

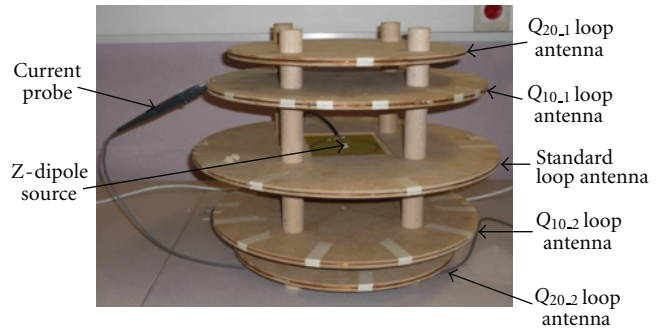

Figure 3: Prototype antenna.

Based on the multipole expansion of the magnetic field, the relationship between the fluxes across the surface delimited by the "sensors set" and the Q_{nm} components of the expansion can be directly obtained [14, 15]. The quasi-static approximation was adopted, and, for the maximum frequency of 30 MHz, it is valid for a $r_M \leq 1.7$ m. In our case, assuming the expansion limited to the second order and in the z-direction ($m = 0$), we have [15]

$$\begin{aligned} Q_{10} &= \frac{10^8 r_M}{32\pi} (\varphi_{10_1} + \varphi_{10_2}), \\ Q_{20} &= \frac{6125 * 10^4 r_M^2}{3\pi\sqrt{21}} (\varphi_{20_1} - \varphi_{20_2}), \end{aligned} \quad (6)$$

where φ_{nm} corresponds to the flux through the loop antenna given by Figure 3. Thus, for the loop configuration given by the same figure, the fluxes through the sensors due to a multipole source will be determined based on the current measured on each loop, after taking into account the magnetic coupling effects of the loops and applying the corresponding antenna factors (AF_{nm}) for $i = 1, 2$:

$$\begin{aligned} \varphi_{10\_i} &= AF_{10} i_{10\_i}, \\ \varphi_{20\_i} &= AF_{20} i_{20\_i}. \end{aligned} \quad (7)$$

The correction of the magnetic coupling between the loop sensors, which can be considered as a postprocessing in the identification procedure, is treated as follows: the total concatenated magnetic flux in each loop can be expressed as the sum of the flux produced by the multipole source (desired) and the fluxes produced by all the other antenna loops (undesired). The measured current in loop n is denoted as $i_{\text{MES}}^{(n)}$ and can be obtained by the following expression:

$$i_{\text{MES}}^{(n)} = i_{\text{DUT}}^{(n)} - \sum_{\substack{k=1 \\ k \neq n}}^{5} \frac{j\omega M_{kn} i_{\text{MES}}^{(k)}}{r_n + j\omega L_n}, \quad (8)$$

where r_n is the resistance and L_n is the self-inductance of the loop n, M_{kn} is the mutual inductance between loops k and n, ω is the angular frequency, and $i_{\text{DUT}}^{(n)}$ is the current in loop n due to the multipole source only.

Thus, considering now the measured currents for all the five loops, one can write (8) in matrix form, solved for $i_{\mathrm{DUT}}^{(n)}$:

$$[i_{\mathrm{DUT}}]_{n,1} = [M]_{n,n}[i_{\mathrm{MES}}]_{n,1}. \tag{9}$$

The elements of $[M]_{n,n}$ are unitary in the diagonal and given by $(j\omega M_{kn}/(r_n + j\omega L_n))$ otherwise. The coefficients Q_{10} and Q_{20} can then be determined by (6), and (7) utilizing the set of currents in (9). This procedure was validated numerically and experimentally, and the results are presented in the following section.

4. Multipole Identification Results

A vector network analyzer (VNA) and large bandwidth current probes were utilized to measure the current ratio of each sensor loop relative to the source, in dB. The frequency range of all experiments was from 20 kHz to 10 MHz.

Three different magnetic field sources were studied: a dipole, a quadrupole, and a generic power transformer. The accuracy of the methodology can be easily verified for the first two sources by utilizing the following expressions:

$$\begin{aligned} &\text{Dipole: } Q_{10} = \pi r^2 i;\ Q_{20} = 0, \\ &\text{Quadrupole: } Q_{10} = 0;\ Q_{20} = \pi r^2 h_0 i, \end{aligned} \tag{10}$$

where r is the radius of the loop and h_0 is the distance between the loops in the quadrupole source. Moreover, for these 2 sources, it is only necessary to present the results for the upper (or lower) loop antennas due to the symmetry on the z-axis with respect to the origin.

The accuracy of the coefficients Q_{10} and Q_{20} of the power transformer can be verified indirectly by calculating [16] and measuring its mutual inductance with a known circular loop and then comparing these results. The VNA and the probes are again used for the measurement.

4.1. Dipole. The measured current ratios loop/source for a dipole of radius 5 cm aligned in the z-axis for the loop sensors Q_{10_1} (loop 2) and Q_{20_1} (loop 1) are presented in Figures 4 and 5, respectively. For each figure, there are 6 curves, in which the 3 upper ones correspond to the lower ones after applying the postprocessing described previously.

Supposing a current of 1 A_{rms} in this dipole and the symmetry in the z-axis and utilizing the plots in Figures 4 and 5, we can determine the 4 currents of (7) and finally the components Q_{10} and Q_{20} with (6).

4.2. Quadrupole. The measured current ratios for a quadrupole of parameters r and h_0 both equal to 5 cm are presented in Figures 6 and 7 in a similar fashion done for the dipole.

4.3. Power Transformer. The measured current ratios loop/source for a power transformer rated 220 V—20 A are presented in Figure 8. The experiment was conducted in a similar manner to the previous ones, although there is no longer symmetry in the z-axis.

The components of the multipole expansion of the dipole, the quadrupole, and the transformer and the errors of the first two sources relatively to (10) are presented in Table 1. The frequency considered for these results was 200 kHz, located on the flat part of the measured curves.

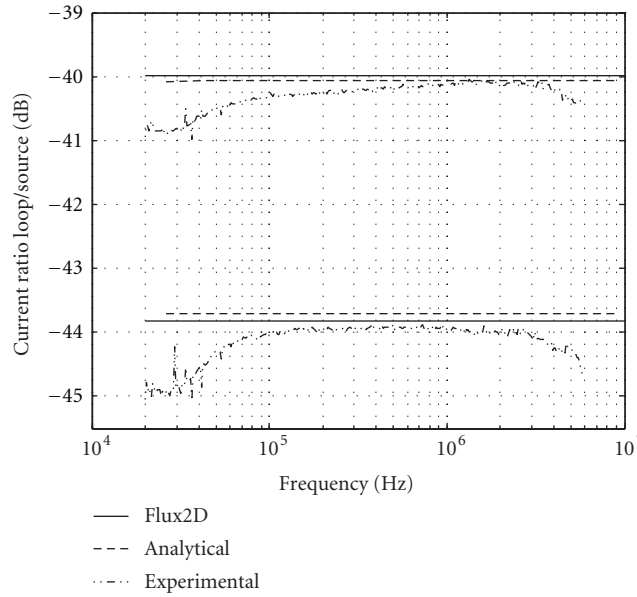

Figure 4: Dipole dB current ratio, sensor Q_{10_1} (loop 2).

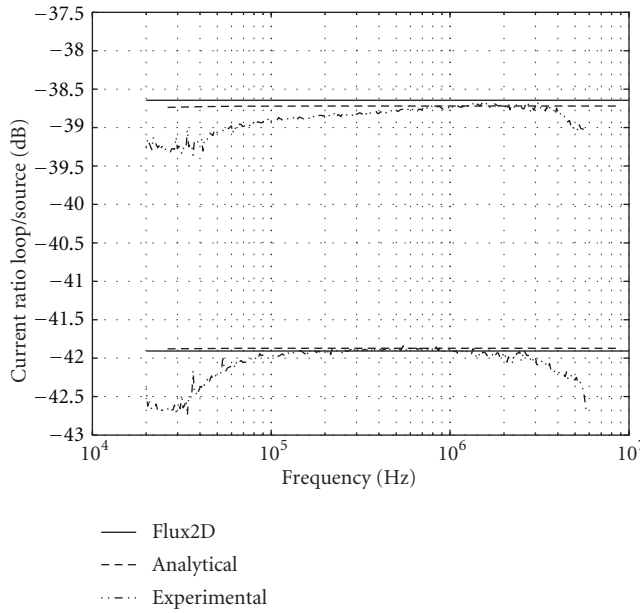

Figure 5: Dipole dB current ratio, sensor Q_{20_1} (loop 1).

Table 1: Components of the multipole expansion.

Component	Q_{10} (m·Am^2)	Q_{20} (m·Am^3)	Error (%)
Dipole	7.3	0	7.6 (Q_{10})
Quadrupole	0	0.63	20 (Q_{20})
Transformer	66.5	0.82	—

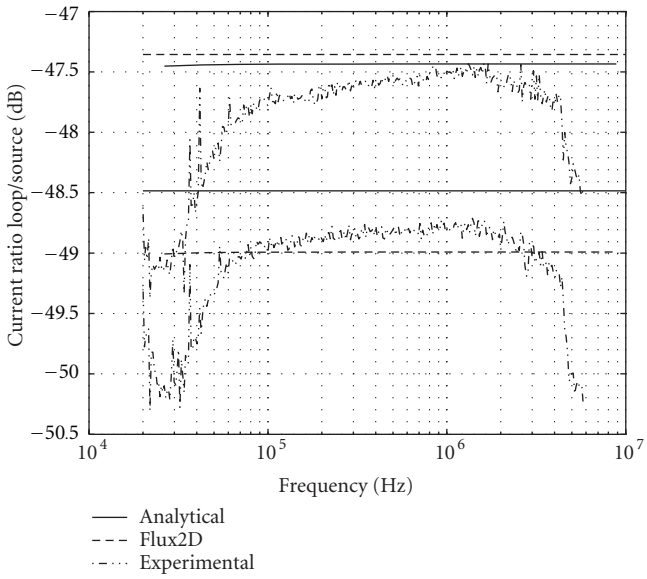

Figure 6: Quadrupole dB current ratio, sensor Q_{10_1} (loop 2).

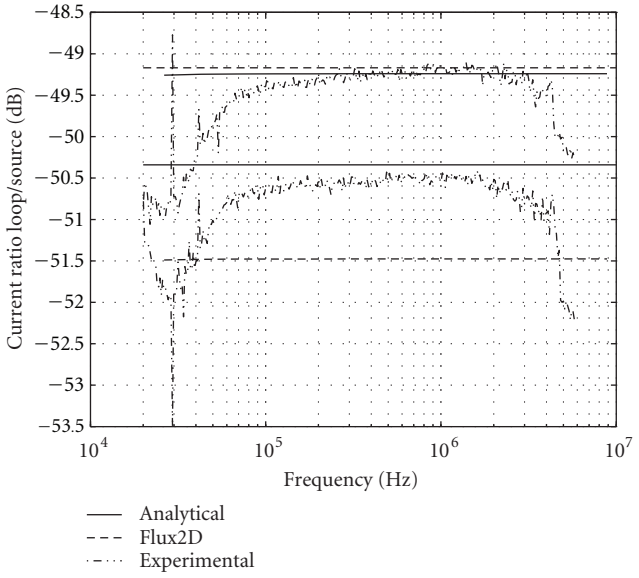

Figure 7: Quadrupole dB current ratio, sensor Q_{20_1} (loop 1).

It should be noted that there is a -4 dB and -3.5 dB difference between the current ratios in Figure 4 and in Figure 5, respectively. Therefore, the effect of the mutual inductances in the antenna would correspond to a difference of 37% and 33% in the calculation of Q_{10} and Q_{20}, respectively, for the dipole.

The mutual inductance between this transformer and a loop can be determined by the following expression:

$$M_{12}i_1 = L_2 i_2, \tag{11}$$

where M_{12} is the mutual inductance, i_1 the current in the transformer, L_2 the self-inductance of the loop, and i_2 the current in the loop.

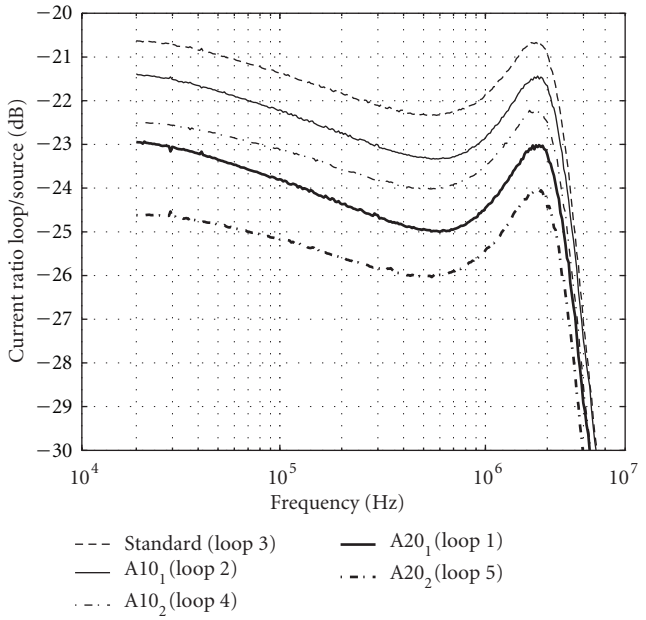

Figure 8: Transformer dB current ratio for all sensor loops.

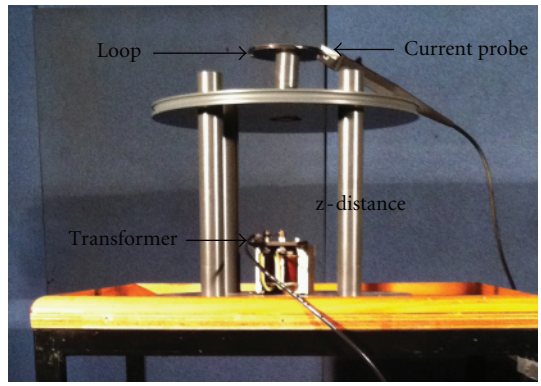

Figure 9: Mutual inductance measurement.

This was done by measuring the ratio of currents using the VNA and applying an analytical formula for the self-inductance of a loop [16] as shown in (11). Figure 9 shows the measurement setup for this case.

5. Computing the Mutual Inductance

Using the equivalent radiated field source model, we can determine the coupling between two equivalent sources through the computation of the mutual inductance. Figure 10 illustrates the configurations regarding the representation of two radiating sources (models 1 and 2).

The computation of the mutual impedance between source 1 and source 2 can be expressed in terms of the electrical field **E** and magnetic field **H** for each source [12]:

$$Z_{12} = -\frac{1}{i_1 i_2} \iint_{\Sigma_1} (\mathbf{E_1} \times \mathbf{H_2} - \mathbf{E_2} \times \mathbf{H_1}). \tag{12}$$

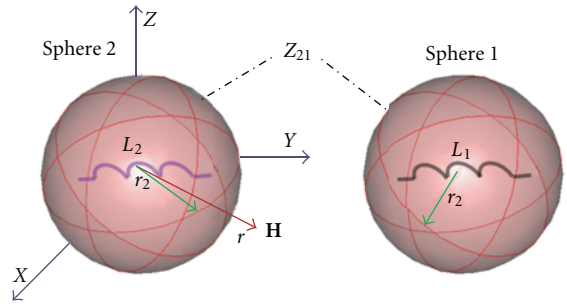

Figure 10: Representation of two radiating sources.

When the spheres that contain the sources do not intersect each other, the mutual impedance can be expressed according to the coefficients of the multipole expansion:

$$Z_{12} = \frac{1}{i_1 i_2}\frac{1}{k^2}\sqrt{\frac{\varepsilon_0}{\mu_0}}\sum_{n=1}^{N_{\max}}\sum_{m=-n}^{n}(-1)^m(Q_{1n,-m} * Q_{2n,m}). \tag{13}$$

The expression of the mutual inductance is

$$M_{12} = \frac{1}{j\omega i_1 i_2}\frac{1}{k^2}\sqrt{\frac{\varepsilon_0}{\mu_0}}\sum_{n=1}^{N_{\max}}\sum_{m=-n}^{n}(-1)^m(Q_{1n,-m} * Q_{2n,m}), \tag{14}$$

where i_1 and i_2 are, respectively, the current that flows in sources 1 and 2, and k is the phase constant.

The coefficients associated to the magnetic transverse modes of the multipole expansion of sources 1 and 2 must be expressed in the same reference: a translation is required, for example, the coefficients of the source 2 can be expressed in the reference of the source 1.

The rotation of the coefficients Q_{nm} is expressed by using Euler angles. It should be mentioned that only two angles are necessary because of the spherical symmetry. The details of the methodology for determining the rotation matrices for complex or real coefficients Q_{nm}, are presented in [17, 18]. The translation is based on the "Addition Theorem for Vector Spherical Harmonics" [18].

The addition theorem links the harmonics evaluated on r to those evaluated on r', where r is measured from the origin of the second spherical basis, whose axes are parallel to the first as shown in Figure 11. The origin of the second spherical basis is located in the first by r''. These 3 vectors are connected by the relation $r = r' + r''$.

The expression of the translation coefficients Q_{snm} are:

$$\begin{aligned} Q^{\mathrm{TE}}_{n'm'} &= \sum_{n=1}^{\infty}\sum_{m=-n}^{n} Q^{\mathrm{TE}}_{mn}\, A_{n',m',n,m} + Q^{\mathrm{TM}}_{nm}\, B_{n',m',n,m}, \\ Q^{\mathrm{TM}}_{n'm'} &= \sum_{n=1}^{\infty}\sum_{m=-n}^{n} Q^{\mathrm{TM}}_{nm}\, A_{n',m',n,m} + Q^{\mathrm{TE}}_{mn}\, B_{n',m',n,m}. \end{aligned} \tag{15}$$

The coefficients $A_{n',m',n,m}$ and $B_{n',m',n,m}$ involve computing of the Wigner $3j$ symbol according to quantum mechanics [19].

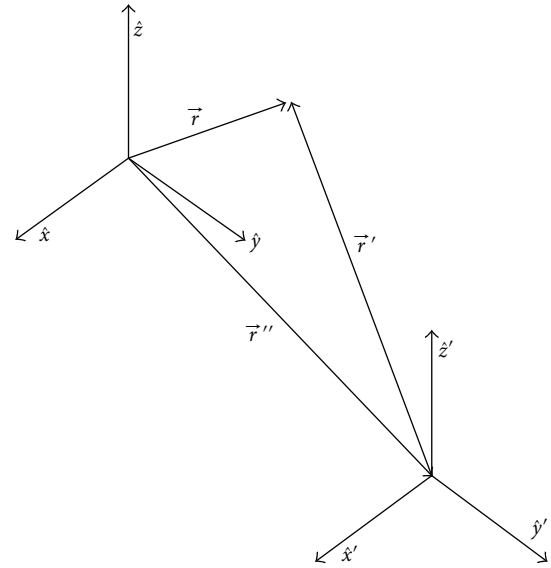

Figure 11: Translation of a spherical basis.

Table 2: Comparison between mutual inductances.

Height (cm)	Measured (nH)	Estimated (nH)	Error (%)
29.3	3.65	3.17	13
35.8	1.98	1.92	3

Utilizing the Q_{10} and Q_{20} of the transformer, it is also possible to estimate its mutual inductance with the loop in a simpler manner. This is achieved by using an analytical expression for the mutual inductance between 2 loops [16], by considering that Q_{10} is represented by a loop and Q_{20} is represented by 2 loops, both in the z axis. These results are presented in Table 2.

6. Conclusion

The presented methodology enables the evaluation of coupling parameters of components by using equivalent emission sources. This method is composed by two steps. At first, the equivalent sources which represent the radiated field component using the multipole expansion representation are identified. It can be obtained by a numerical or an experimental approach. Both of them were discussed in the paper. Secondly, the equivalent sources will be used to compute the coupling between them, which was represented by a mutual inductance as a function of the distance that separates them.

Other kind of multipole expansions like the cylindrical one can be more suitable for modeling components such as tracks or cables, and it will also be considered. For example, in the case of the coupling between a track and a component, the spherical harmonics method is not very adequate and other harmonics method should be used.

The method proposed could be helpful when used together with other circuit simulator methods in the evaluation of equivalent circuit of power electronics devices (R-L-M-C). This will give us a considerable gain of memory space

concerning the full model configuration used in EMC filter numerical simulations.

References

[1] R. Redl, "Electromagnetic environmental impact of power electronics equipment," *Proceedings of the IEEE*, vol. 89, no. 6, pp. 926–938, 2001.

[2] R. Redl, "Power electronics and electromagnetic compatibility," in *Proceedings of the 27th Annual IEEE Power Electronics Specialists Conference (PESC '96)*, vol. 1, pp. 15–21, January 1996.

[3] E. Hoene, "EMC in Power Electronics," in *Proceedings of the 5th International Conference on Integrated Power Systems (CIPS '08)*, pp. 1–5, March 2008.

[4] A. R. Ruddle, X. Ferrières, J. P. Parmantier, and D. D. Ward, "Experimental validation of time-domain electromagnetic models for field coupling into the interior of a vehicle from a nearby broadband antenna," vol. 151, no. 6, pp. 430–433.

[5] D. S. Dixon, M. Obara, and N. Schade, "Finite-element analysis (FEA) as an EMC prediction tool," *IEEE Transactions on Electromagnetic Compatibility*, vol. 35, no. 2, pp. 241–248, 1993.

[6] S. Zangui, K. Berger, C. Vollaire, E. Clavel, R. Perrussel, and B. Vincent, "Modeling the near-field coupling of EMC filter components," in *Proceedings of the IEEE International Symposium on Electromagnetic Compatibility*, pp. 825–830, July 2010.

[7] S. Zangui, K. Berger, B. Vincent et al., *Evaluation of Coupling Parameters of EMC Filter Components by Using Equivalent Emission Sources*, MOMAG, Brazil, 2010.

[8] S. Zangui, K. Berger, R. Perrussel, E. Clavel, C. Sartori, and C. Vollaire, *Using Equivalent Emission Sources to Evaluate the Coupling between Components*, Compumag, Sydney, Australia, 2011.

[9] S. Zangui, B. Vincent, K. Berger et al., "Near-field coupling between EMC filter components," in *Proceedings of the 14th Biennial IEEE Conference on Electromagnetic Field Computation (CEFC '10)*, vol. 1, pp. 9–12, May 2010.

[10] A. E. Ruehli, "Equivalent circuit models for three-dimensional multiconductor systems," *IEEE Transactions on Microwave Theory and Techniques*, vol. 22, no. 3, pp. 216–221, 1974.

[11] S. Zangui, B. Vincent, K. Berger, E. Clavel, R. Perrussel, and C. Vollaire, *Equivalent Source Corresponding to Radiated Field of EMC Filter Components*, EMC Europe, Wroclaw, Poland, 2010.

[12] B. C. Brock, "Using vector spherical harmonics to compute antenna mutual impedance from measured or computed fields," SANDIA Report, 2001.

[13] A. Gati, Y. Adane, M.-F. Wong, J. Wiart, and V. Fouad-Hanna, "Inverse characterization of antennas by equivalent sources using spherical harmonics," *Comptes Rendus Physique*, vol. 6, no. 6, pp. 640–646, 2005.

[14] B. Vincent, O. Chadebec, J. L. Schanen, and K. Berger, "Loop antennas for near-field multipolar-expansion identification: first experimental validations," *IEEE Transactions on Instrumentation and Measurement*, vol. 59, no. 12, pp. 3086–3092, 2010.

[15] B. Vincent, O. Chadebec, J.-L. Schanen et al., "New robust coil sensors for near field characterization," *Journal of Microwaves and Optoelectronics*, vol. 8, no. 1, pp. 64S–77S, 2009.

[16] E. Durand, *Magnétostatique*, Masson et Cie Editeurs, 1968.

[17] M. A. Blanco, M. Flórez, and M. Bermejo, "Evaluation of the rotation matrices in the basis of real spherical harmonics," *Journal of Molecular Structure: THEOCHEM*, vol. 419, no. 1–3, pp. 19–27, 1997.

[18] C. A. Balanis, *Advanced Engineering Electromagnetics*, John Wiley & Sons, New York, NY, USA, 1989, chapter 10.

[19] A. Messiah, "Clebsch-Gordan (C.-G.) Coefficients and "3j" Symbols," in *Appendix C.I in Quantum Mechanics*, vol. 2, pp. 1054–1060, North-Holland, Amsterdam, The Netherlands, 1962.

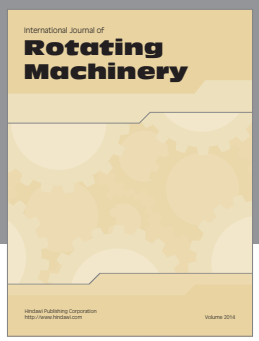

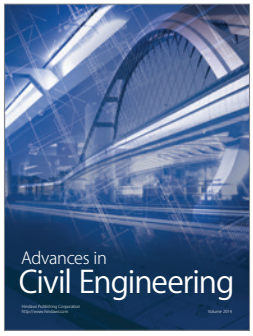

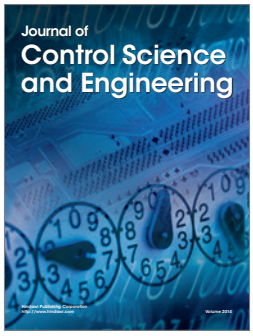

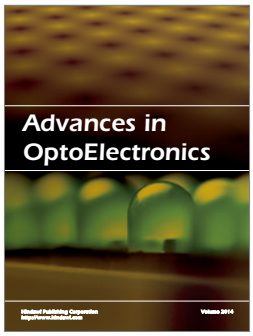

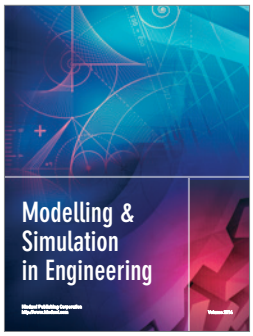

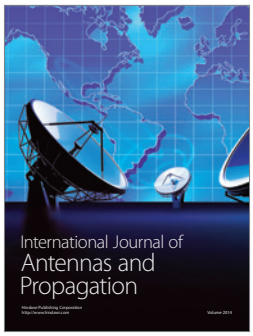

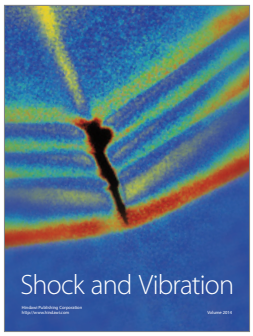

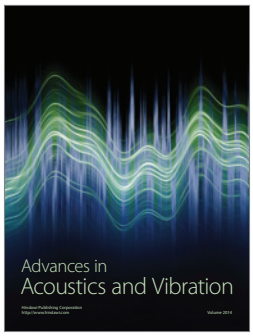

Hindawi

Submit your manuscripts at
http://www.hindawi.com